Supplementary Information (SI) for Soft Matter.

Supporting Information

Dispersions of Weakly Charged Thermoresponsive Microgels at High Densities

M. Hildebrandt,[a] D. Pham Thuy,[a] A. Domgans,[a] A. Scotti,[b] S. Prévost,[c] M. Adhikari,[d] J. Horbach,[d] M. Karg[a,e]*

[a]Institut für Physikalische Chemie I: Kolloide und Nanooptik, Heinrich-Heine-Universität Düsseldorf, Universitätsstraße 1, 40225 Düsseldorf, Germany

[b]Division of Physical Chemistry, Lund University, SE-22100 Lund, Sweden

[c]Institut Laue-Langevin - 71 avenue des Martyrs CS 20156, 38042 GRENOBLE Cedex 9 – France

[d]Institut für Theoretische Physik II: Weiche Materie, Heinrich-Heine-Universität Düsseldorf, Universitätsstraße 1, 40225 Düsseldorf, Germany

[e]Institute of Chemistry, Physical Chemistry of Functional Polymers, Martin Luther University Halle-Wittenberg, 06120 Halle (Saale), Germany
E-Mail: matthias.karg@chemie.uni-halle.de

Transmission Electron Microscopy (TEM)

In order to verify the core-shell (CS) nature of our microgels we performed TEM. As seen in **Figure S1a** and **b,** the microgels possess single cores homogeneously encapsulated in polymer shells. Due to the difference in electron density, the CS structure is clearly visible. The fraction of core-less microgels (an example is highlighted by a red circle in **Figure S1b** is below 1% and therefore considered negligible. From these and additional TEM images we determined average core radii of 18 ± 2 nm. The size distribution of the SiO_2 cores is shown in **Figure S1c**.

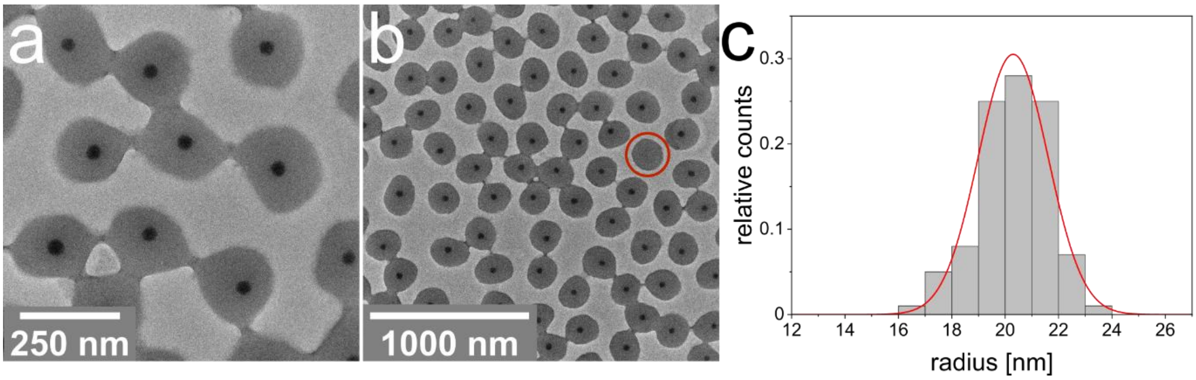

Figure S1. Brightfield TEM images of CS1 (**a**, **b**) at different magnifications. The red circle in (**b**) highlights a microgel without core. (**c**) Respective size distribution of the SiO_2 cores with a Gaussian fit (red line). TEM images and the respective size distribution were adapted from our previous work.[1]

Zeta Potential

The temperature-dependent zeta potentials of the CS microgels are shown in **Figure S2**. The zeta potential was calculated based on the Smoluchowski approximation using the measured electrophoretic mobilities. At low temperatures, the CS microgels (salt-free) exhibit a zeta potential of -17 mV which decreases after passing a temperature of 35 °C, resulting in a final potential of -28 mV at 50 °C. This negative charge is solely related to the anionic radical initiator used in the seeded precipitation polymerization. As expected, the charge of the CS microgels increases when the microgels deswell, i.e. temperature is increased leading to a reduction of surface area and therefore an increase in charge density.

In 0.5 mM KCl the zeta potential is decreased to -3 mV at 20 °C indicating pronounced charge-screening due to the increased ionic strength. For an increase in temperature, we can see the same trend as for the salt-free sample. The sample with salt has a zeta potential of -18 mV at 50 °C, i.e. in the collapsed state of the CS microgels.

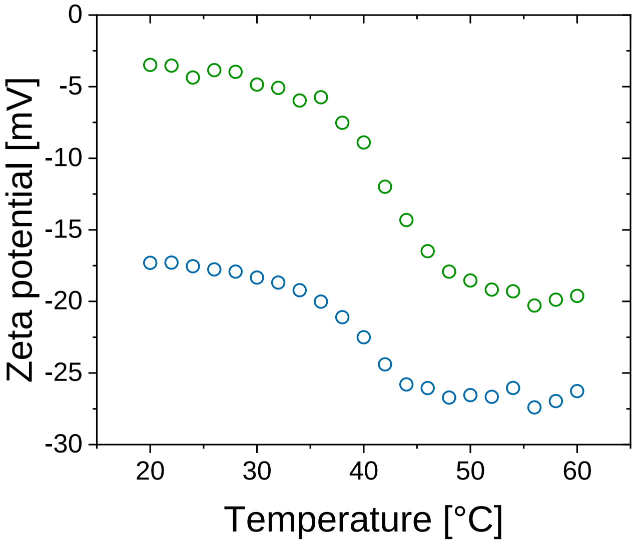

Figure S2. Zeta potentials of CS microgels in absence (blue symbols) and presence of KCl (green symbols) as a function of temperature.

Form Factor Modeling and Fitting

We performed SAXS and SANS experiments on dilute and concentrated aqueous dispersions of the CS microgels. The scattering data was radially averaged to obtain the scattering intensity *I*, as function of the magnitude of the scattering vector $\vec{q}$:

$$|\vec{q}| = q = \frac{4\pi}{\lambda} sin\frac{\theta}{2} \tag{S1}$$

Here, the wavelength of the respective X-ray or neutron beam is given by *λ* and the scattering angle is given by *θ*.

Generally, the scattering intensity can be expressed by:

$$I(q) = NV_{\mathrm{particle}}{}^{2}\Delta SLD^{2}P(q)S(q) + I_{\mathrm{B}} \tag{S2}$$

Here, *N* is the particle number density, V_{particle} is the volume of the scattering object and *ΔSLD* is the difference in scattering length density (SLD) between the scattering object and the solvent. With the form factor *P*(*q*) of the scattering object and the structure factor S(*q*). In order to describe additional background contributions I_{B} is added.

For dilute dispersions, the structure factor contributions become neglectable as $S(q) \approx 1$.

In order to describe the scattering intensity, $I(q)$ of the CS microgels we made use of core-shell model:

$$I(q) = \frac{scale}{V_{\mathrm{particle}}}\left[3V_{core}SLD_{\mathrm{core}}k(qR_{\mathrm{core}}) + 3V_{particle}SLD_{\mathrm{shell}}k\left(qR_{\mathrm{particle}}\right) - 3V_{core}SLD_{\mathrm{shell}}k(qR_{\mathrm{core}}) - 3V_{\mathrm{particle}}SLD_{\mathrm{solvent}}k\left(qR_{\mathrm{particle}}\right)\right]^2 + I_{\mathrm{B}} \qquad \text{(S3)}$$

with

$$k(qR) = \frac{\sin(qR) - qR\cos(qR)}{(qR)^3}$$

Here, *scale* corresponds to a scaling factor (representing the volume fraction if measured in absolute units), V is the volume of the respective scattering object and R_{core} and R_{particle} are attributed to the total radii of the core and the particle. Here, R_{particle} is the defined by the sum of thickness of the shell $\Delta t_{\mathrm{shell}}$ and R_{core}. As the core and the solvent possess a homogeneous structure, we kept the *SLD* constant for both materials. $k(qR)$ corresponds to the form factor oscillations of a spherical scattering object.

In the swollen state (20 °C), the *SLD* of the microgel shell is described with an exponential decay in the *SLD* profile of the shell to ascribe for the gradient in crosslinker density (core-exponential-shell model).[2]

For the CS microgels in their collapsed state (45 °C) the shell is described with a homogeneous shell and therefore, the *SLD* of the shell is kept constant (core-homogeneous-shell model).

More details to the fitting procedure and the applied core-shell models are given in the Supporting Information of our previous work on the same CS microgels.[1]

In order to fit the high q ($q > 0.3$ nm^{-1}) SANS data, recorded from CS microgels in their swollen state (20 °C), a Lorentzian function (Ornstein-Zernike contribution) was added to describe internal fluctuations of the polymer network.

$$I(q) = \frac{I_0}{1 + q^2 {\xi_{OZ}}^2} \qquad \text{(S4)}$$

Here, I_0 is the forward scattering and ξ_{OZ} corresponds to the correlation length.

The scattering intensity of the silica cores without polymer shell is described with a simple polydisperse sphere model.

$$I(q) = \frac{scale}{V_{\text{particle}}}\left[3V(R)\Delta SLD\,\frac{\sin(qR) - qR\cos(qR)}{(qR)^3}\right]^2 + I_{\text{B}} \quad \text{(S5)}$$

In order to take the polydispersity of the particles into account, we applied a gaussian distribution on the radius and therefore the volume of the scattering object in the form factor model used to fit the scattering profiles. Here, $\langle R\rangle$ is the average particle radius and σ_{poly} corresponds to the relative size polydispersity.

$$D\left(R, \langle R\rangle, \sigma_{\text{poly}}\right) = \frac{1}{\sqrt{2\pi\sigma_{\text{poly}}{}^2}}\,exp\left(-\frac{(R-\langle R\rangle)^2}{2\sigma_{\text{poly}}{}^2}\right) \quad \text{(S6)}$$

The form factor fitting was performed with the SasView[3] software and the respective parameters are listed in **Tables S1** and **S2**. For details about the fitting procedure of the SAXS data we refer to our previous work.[1] The fitting process of the SANS/SLS data is explained in the respective section of the SI. Please note that the Gaussian size distribution of the cores (σ_{core}) needed to be fixed to the value of 0.1 due to its weak contribution to the overall scattering profiles.

Table S1. Parameters applied to fit the SAXS and merged SANS/SLS profiles of the dilute CS microgels in aqueous dispersion in absence of salt. Parameters for SAXS are adapted from our previous work.[1]

Parameters	**[1]SAXS (20°C)**	**[2]SANS/SLS (20°C)**	**[3]SANS/SLS (45°C)**
scale	0.029	0.03	0.006
IB [a. u.]	0.2	0.057	0.061
I_0 [a. u.]	-	0.12	-
ξ_{OZ} [nm]	-	3.2	-
R_{core} [nm]	18	18	18
Δt_{shell} [nm]	120	120	70
SLD_{core} [10^{-6} Å^{-2}]	17.75	3.3	3.3
$SLD_{\text{shell, in}}$ [10^{-6} Å^{-2}]	9.89	5.0	3.4
$SLD_{\text{shell, out}}$ [10^{-6} Å^{-2}]	9.43	6.4	3.4
SLD_{solvent} [10^{-6} Å^{-2}]	9.43	6.4	6.4
σ_{core}	0.1	0.1	0.1
σ_{shell}	0.1	0.09	0.08
A	2.2	2.4	-

[1] Core-exponential-shell model
[2] Core-exponential-shell model + Ornstein-Zernike contribution
[3] Core-homogeneous-shell model

Table S2. Parameters applied to fit the SAXS and merged SANS/SLS profiles of the dilute CS microgels in aqueous dispersion with salt.

Parameters	**[1]SAXS (20°C)**	**[2]SANS/SLS (20°C)**	**[3]SANS/SLS (45°C)**
scale	0.029	0.027	0.005
IB [a. u.]	0.2	0.057	0.061
I_0 [a. u.]	-	0.13	-
ξ_{OZ} [nm]	-	3.2	-
R_{core} [nm]	18	18	18
Δt_{shell} [nm]	120	118	71
SLD_{core} [10^{-6} Å^{-2}]	17.75	3.3	3.3
$SLD_{\text{shell, in}}$ [10^{-6} Å^{-2}]	9.89	5.0	3.3
$SLD_{\text{shell, out}}$ [10^{-6} Å^{-2}]	9.43	6.4	3.3
SLD_{solvent} [10^{-6} Å^{-2}]	9.43	6.4	6.4
σ_{core}	0.1	0.1	0.1
σ_{shell}	0.1	0.08	0.08
A	2.2	2.3	-

[1] Core-exponential-shell model
[2] Core-exponential-shell model + Ornstein-Zernike contribution
[3] Core-homogeneous-shell model

The volumes of the core and shell in combination with the respective contrast situations in SANS and SAXS based on the difference in SLDs are, are listed in **Table S3.** In addition, the interplay between contrast and volume of the scattering of core and shell, based on **Equation S2,** is listed in the following table. This reveals a dominating contribution of the shell (PNIPAM) to the scattering profile in both contrast situations. The difference is significant in SAXS and SANS but much more expressed for SANS, where the contribution of the core can be nearly neglected. For SAXS the core contribution is still pronounced and visible in the respective SAXS profiles.

Table S3. Influence of the respective SAS contrast and CS microgel dimensions on the scattering properties.

Method	**Material**	$V_{core/shell}$ **[m^3]**	ΔSLD **[10^{-6} Å^{-2}]**	$V^2 \cdot \Delta SLD^2$ **[10^{12} m^2]**
SAXS	SiO_2	2.44E-20	8.32	0.041
	PNIPAM	1.10E-17	0.46	25.530
SANS	SiO_2	2.44E-20	3.1	0.006
	PNIPAM	1.10E-17	1.6	308.860

Figure S3 shows the SAXS profile of a dilute dispersion of CS microgels in their collapsed state, recorded at a temperature of 40 °C. We applied a core-homogenous-shell model on the scattering profile in order to fit the from factor of the CS microgel. The fit is presented as solid red line and is in good agreement with the recorded data. In **Table S4** we show the respective parameters of the fit which are comparable with our results from SANS. For more details we refer to our previous work.[1]

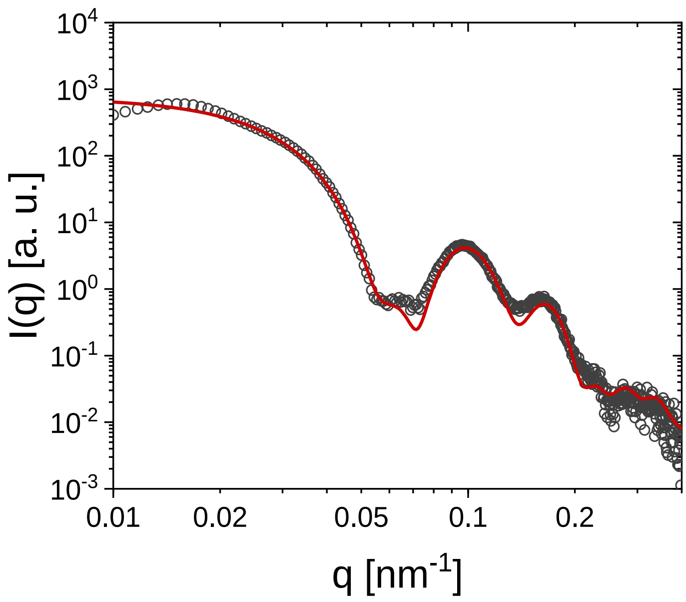

Figure S3. SAXS profile of CS microgels with generalized volume fraction ζ (20 °C) = 0.09 recorded at 40 °C. The solid red line indicates the form factor fit based on a core-homogeneous-shell model. Adapted from our previous work.[1]

Table S4. Parameters of the core-homogeneous-shell model applied to fit the form factor in the SAXS profile of the dilute CS microgels in aqueous dispersion. Adapted from our previous work.[1]

Parameters	**SAXS (40°C)**
scale	2.733
IB [a. u.]	0.003
R_{core} [nm]	18
$\Delta t_{\mathrm{shell}}$ [nm]	72
SLD_{core} [10^{-6} Å^{-2}]	17.75
$SLD_{\mathrm{shell,\ in}}$ [10^{-6} Å^{-2}]	10.3
$SLD_{\mathrm{shell,\ out}}$ [10^{-6} Å^{-2}]	10.3
SLD_{solvent} [10^{-6} Å^{-2}]	9.43
σ_{core}	0.1
σ_{shell}	0.08

Small-Angle Neutron and Static Light Scattering

The recorded SANS profiles were merged with the respective SLS profiles and are shown in **Figure S4a**. Blue symbols correspond to CS-microgel dispersions recorded in absence of salt while the green ones were recorded from samples with salt. Scattering profiles were recorded at temperatures of 20 °C and 45 °C and the dotted, vertical line indicates the boundary between the merged SLS and SANS section of the scattering profile. The form factor fit which is shown by the solid red line is obtained from form factor analysis of the total scattering profile, including the SLS section. In order to take into account the smearing in SANS, the error in *q* was included in the fitting procedure. Due to the very low error in *q* of the merged SLS data, a very small error of 10^{-4} nm^{-1} was assigned to the respective data points to enable from factor analysis in SasView. A core-exponential-shell model and a core-homogeneous-shell model were used to describe the scattering properties of the CS microgels in the swollen (20 °C) and the collapsed (45 °C) state. In the fitting process known parameters like the *SLD*s of the solvent, core and the radius of the core were set to a fixed value and kept constant. The other parameters were approximated, within physically reasonable values to describe the respective scattering profile. Then all non-fixed parameters of the core-shell model were fitted simultaneously.

For the data recorded at 20 °C, the *SLD* of the shell needed to be limited to a value of $5 \cdot 10^{-6}$ Å^{-2}, because otherwise the fit did not sufficiently describe the low q-range of the scattering profile. In case of the scattering profiles recorded at 45 °C, the procedure was comparable, but *scale* was fixed at a value calculated based on the value of *scale* at 20 °C and the radii of the CS microgels at 20 °C and 45 °C. Here, the SLD of the shell was not limited to any borders.

For both salt conditions, the form factor analysis yielded similar results at both temperatures, as presented in **Table S1** and **S2.** For all profiles we find distinct form factor oscillations which are well described by the respective fits and are primarily related to the PNIPAM shell of the CS microgel. For both temperatures we barley detect form factor oscillations corresponding to the SiO_2 core.

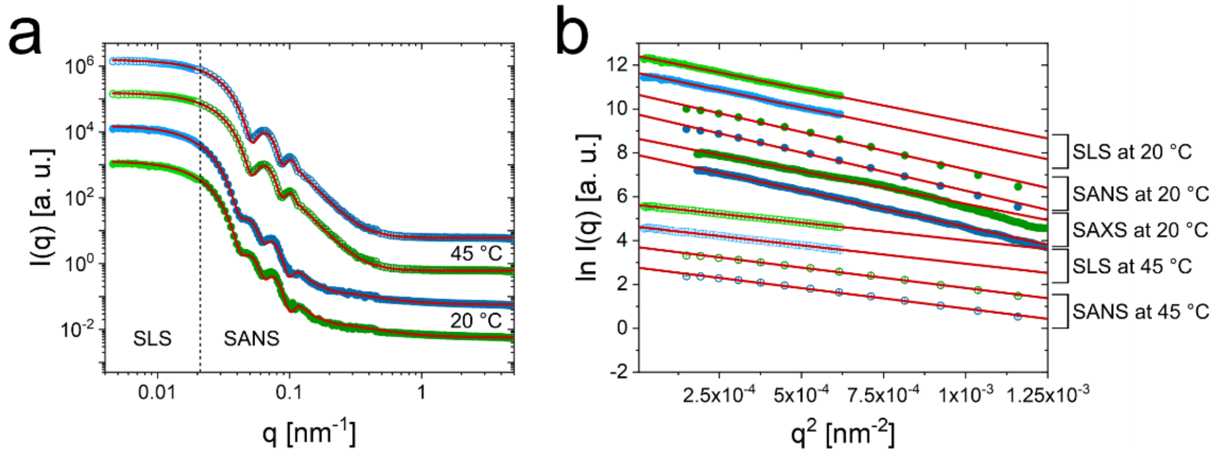

Figure S4. Scattering profiles referring to CS microgels measured in the absence of salt (blue) and the presence of 0.5 mM KCl (green) (**a**) Full *q*-range SANS scattering profiles at 20°C (full symbols) and 45°C (open symbols) with merged scattering profiles from SLS. The solid red lines correspond to the respective form factor fits (core-exponential-shell model for the profiles recorded at 20 °C and core-homogeneous-shell model at 45 °C). (**b**) Guinier plots from the low *q*-range (scattering of the shell) for SLS, SANS and SAXS. Plots are shifted on the y-axis for the sake of clarity.

In addition to the form factor analysis, we performed Guinier-analysis on the plateau like section of the scattering profiles related to the scattering of the CS microgel shells. The Guinier plots are shown in **Figure S4b** including the linear fits to the data. We find a sufficient agreement between the fits and the respective data points. The results from the Guinier analysis are presented in **Table S5**.

The linearized Guinier equation is shown below:

$$\ln(I(q)) = \ln(I_0) - \frac{q^2 {R_g}^2}{3} \tag{S7}$$

With q, the scattering vector, I_0 being the scattering intensity at infinitely small q and the radius of gyration R_g. We obtained radii of gyration between 95 and 102 nm at 20°C and between 70 and 75 nm at 45°C. In general, values of R_g from samples with KCl are slightly smaller than without salt. The radii of gyration obtained from different scattering techniques are in good agreement with each other and proof the reliability of the results independent of the respective contrast.

Table S5. Results from Guinier analysis.

Method	**C_{KCl} [mM]**	**Temperature [°C]**	**Slope [nm^2]**	**R_g [nm]**
SAXS	0	20	-3272 ± 6	99.1 ± 0.2
SAXS	0.5	20	-2969 ± 15	94.4 ± 0.5
SANS	0	20	-3483 ± 61	102.2 ± 1.8
SANS	0.5	20	-3405 ± 78	101.1 ± 2.3
SANS	0	45	-1869 ± 34	74.9 ± 1.4
SANS	0.5	45	-1863 ± 29	74.8 ± 1.2
SLS	0	20	-3148 ± 23	97.2 ± 0.7
SLS	0.5	20	-3008 ± 16	95.0 ± 0.5
SLS	0	45	-1680 ± 7	71.0 ± 0.3
SLS	0.5	45	-1610 ± 8	69.5 ± 0.3

Comparison of the Generalized Volume Fractions

Table S6. R_h and the respective ζ for CS microgels at 20 °C and 40 °C.

T = 20 °C **c_{KCl} = 0 mM**	**T = 20 °C** **c_{KCl} = 0.5 mM**	**T = 40 °C** **c_{KCl} = 0 mM**	**T = 40 °C** **c_{KCl} = 0.5 mM**
147 nm	145 nm	103 nm	101 nm
0.42	0.40	0.14	0.14
0.56	0.54	0.19	0.18
0.70	0.67	0.24	0.23
0.84	0.81	0.29	0.27

Scattering Pattern in the Fluid Phase at 40 °C

SAXS patterns of CS microgel dispersions with generalized volume fractions ζ (20 °C) of 0.42, 0.56, 0.70 and 0.84 were recorded at a temperature of 40 °C. The increase in temperature leads to a reduction in ζ and therefore the scattering patterns no longer exhibit Bragg peaks but a distinct fluid structure factor. This is presented in **Figure S5**, where all CS microgel dispersions feature an isotropic scattering pattern over a broad range of ζ between 0.14 and 0.29. Compared to the scattering patterns recorded in the absence of salt (top row), the structure factors are much broader and less intense in the presence of salt (bottom row). This is a first indicator that the addition of salt decreases the effective range of inter particle interactions at the probed temperature.

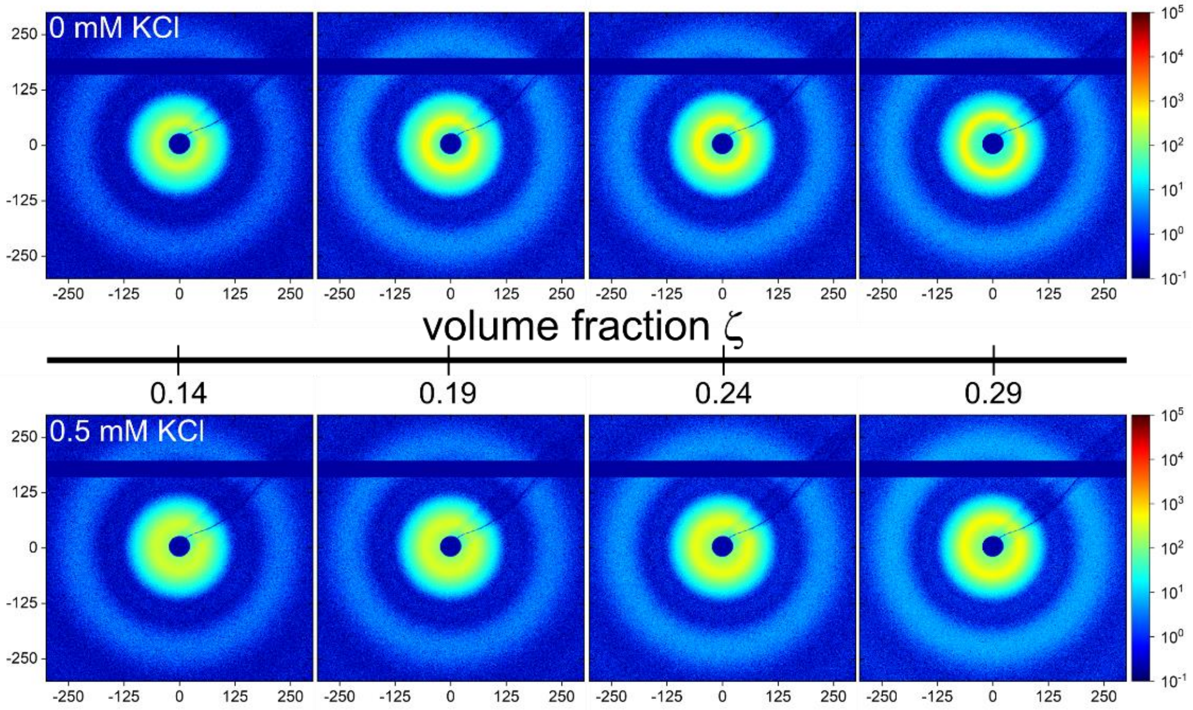

Figure S5. SAXS pattern of CS microgels in absence (top) and in presence of salt (bottom) with increasing generalized volume fraction ζ (T = 40 °C). ζ is calculated based on number concentration *N* and the hydrodynamic radius at 40 °C measured in the absence of KCl.

Form Factor Modeling in Dense Packings at 20 °C

Due to the presence of distinct form factor oscillations in the SAXS profiles of the CS microgels in dense packings, we were able to model form factors describing the scattering of the shell, even when $S(q) \neq 1$. The modeled form factors are presented in **Figure 4a** in the main manuscript and the respective parameters are listed in **Tables S7** and **Table S8**. For CS microgel dispersions with similar number concentrations, the same parameters could be applied on the scattering profiles recorded from samples in absence and presence of salt.

Table S7. Parameters used for the form factor modeling (core-exponential-shell model) of the CS microgel dispersions in the concentrated regime in absence of salt. ζ is calculated based on number concentration *N* and the hydrodynamic radius at 20 °C in the salt-free state. Adapted from our previous work.[1]

Parameters	**ζ (20 °C) = 0.42**	**ζ (20 °C) = 0.56**	**ζ (20 °C) = 0.70**	**ζ (20 °C) = 0.84**
scale	0.28	0.34	0.36	0.39
IB [a. u.]	0.2	0.2	0.2	0.2
R_{core} [nm]	18	18	18	18
$\Delta t_{\mathrm{shell}}$ [nm]	120	116	109	98
SLD_{core} [10^{-6} Å^{-2}]	17.75	17.75	17.75	17.75
$SLD_{\mathrm{shell,\ in}}$ [10^{-6} Å^{-2}]	9.89	9.89	9.89	9.89
$SLD_{\mathrm{shell,\ out}}$ [10^{-6} Å^{-2}]	9.43	9.43	9.43	9.43
SLD_{solvent} [10^{-6} Å^{-2}]	9.43	9.43	9.43	9.43
σ_{core}	0.1	0.1	0.1	0.1
σ_{shell}	0.08	0.08	0.08	0.08
A	2.2	2.6	3.5	4.9

Table S8. Parameters used for the form factor modeling (core-exponential-shell model) of the CS microgel dispersions in the concentrated regime in presence of salt. ζ is calculated based on number concentration *N* and the hydrodynamic radius at 20 °C in the salt-free state.

Parameters	**ζ (20 °C) = 0.42**	**ζ (20 °C) = 0.56**	**ζ (20 °C) = 0.70**	**ζ (20 °C) = 0.84**
scale	0.28	0.34	0.36	0.39
IB [a. u.]	0.2	0.2	0.2	0.2
R_{core} [nm]	18	18	18	18
$\Delta t_{\mathrm{shell}}$ [nm]	120	116	109	98
SLD_{core} [10^{-6} Å^{-2}]	17.75	17.75	17.75	17.75
$SLD_{\mathrm{shell,\ in}}$ [10^{-6} Å^{-2}]	9.89	9.89	9.89	9.89
$SLD_{\mathrm{shell,\ out}}$ [10^{-6} Å^{-2}]	9.43	9.43	9.43	9.43
SLD_{solvent} [10^{-6} Å^{-2}]	9.43	9.43	9.43	9.43
σ_{core}	0.1	0.1	0.1	0.1
σ_{shell}	0.08	0.08	0.08	0.08
A	2.2	2.6	3.5	4.9

Determination of Lattice Constants

Since the crystal structure of the colloidal crystals was determined to be a hexagonally closed packed (hcp) structure, we are able to relate the Bragg peaks to the respective Miller indices.[1] This enables us to determine precisely the lattice constant *a*, based on the linear dependency between the Bragg peak position q_{hkl} and the lattice spacing, as shown in **Figure S6**. The linear dependency is also shown in **Equation S8**.

$$q_{hkl} = \frac{2\pi}{a}\left(\frac{4}{3}\left(h^2 + hk + k^2\right) + \frac{3}{8} l^2\right)^{\frac{1}{2}} \tag{S8}$$

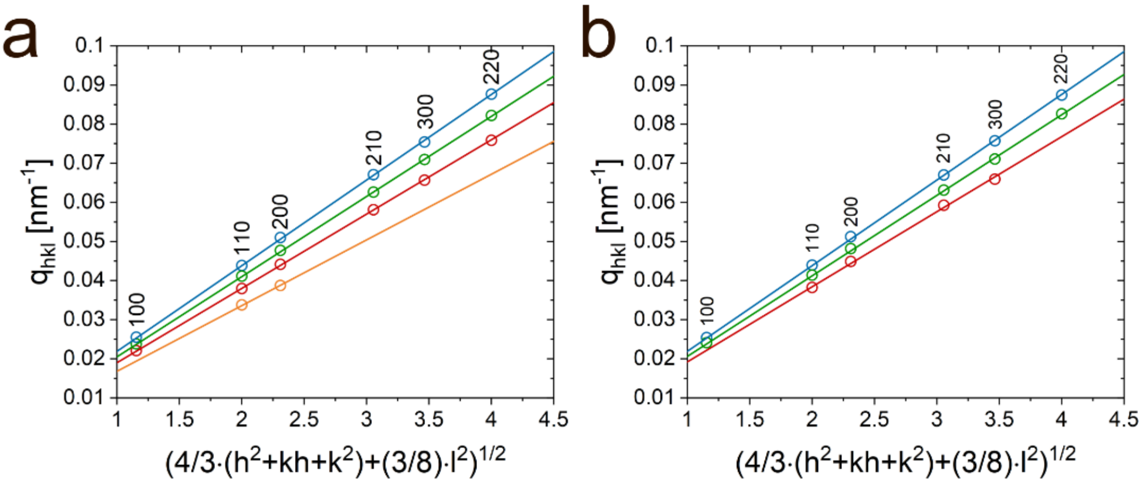

Figure S6. Determination of the lattice constant *a* in absence (**a**) and presence of KCl (**b**). Position of the Bragg peak q_{hkl} as function of $\left(\frac{4}{3}\left(h^2 + hk + k^2\right) + \frac{3}{8} l^2\right)^{\frac{1}{2}}$. Selected Bragg peaks recorded from CS microgel dispersions with ζ = 0.42 (orange circles), 0.56 (red circles), 0.7 (green circles) and 0.84 (blue circles). The straight, solid lines indicate the linear fits applied to the data. ζ is calculated based on number concentration *N* and the hydrodynamic radius at 20 °C in the salt-free state. Figure S6a is adapted from our previous work.[1]

Over a broad range of ζ, independent on the concentration of KCl we see a perfect linear relationship between the position of the Bragg peaks and the respective lattice spacings. For the CS microgel dispersion with ζ = 0.42 in the salt-free state and ζ = 0.56 in the presence of salt only a reduced number of Bragg peaks was used for the extraction of the lattice constant. This is due to weak intensity or interference of the Bragg peak with a structure factor maximum related a fluid-like contribution to the scattering profile. The extracted lattice constants and respective slopes of the fits are presented in **Table S9**. Here the addition of KCl to the CS microgel dispersion has no noticeable influence on the lattice constants of the colloidal crystals. It rather increases the volume fraction at which the system is able to form stable colloidal crystals.

Table S9. Slopes and respective lattice constants *a* obtained from linear fits. ζ is calculated based on number concentration *N* and the hydrodynamic radius at 20 °C in the salt-free state. Data recorded from samples in absence of salt is adapted from our previous work.[1]

ζ (20 °C) / c_{KCl} [mM]	Slope [nm^{-1}]	*a* [nm]
0.42 / 0 mM	0.0168	374
0.42 / 0.5 mM	-	-
0.56 / 0 mM	0.0190	331
0.56 / 0.5 mM	0.0192	327
0.70 / 0 mM	0.0205	306
0.70 / 0.5 mM	0.0206	305
0.84 / 0 mM	0.0219	287
0.84 / 0.5 mM	0.0219	287

Williamson-Hall Analysis

In order to extract the size of the coherently scattering domains of the prepared colloidal crystals, we performed Williamson-Hall analysis on the diffraction pattern. Here, we determined the width of the Bragg peaks in radial and azimuthal orientation as function of the scattering vector *q* as presented in **Figure S7**. From the slope of the linear fit applied on the data we could extract the strain of colloidal crystals $g_{\mathrm{rad/azi}}$ and the size of the coherently scattering domains $L_{\mathrm{rad/azi}}$ based on the respective intercept.

$$w_{rad/azi}{}^2(q) = \left(\frac{2\pi}{L_{rad/azi}}\right)^2 + g_{rad/azi}\, q^2 \qquad \text{(S9)}$$

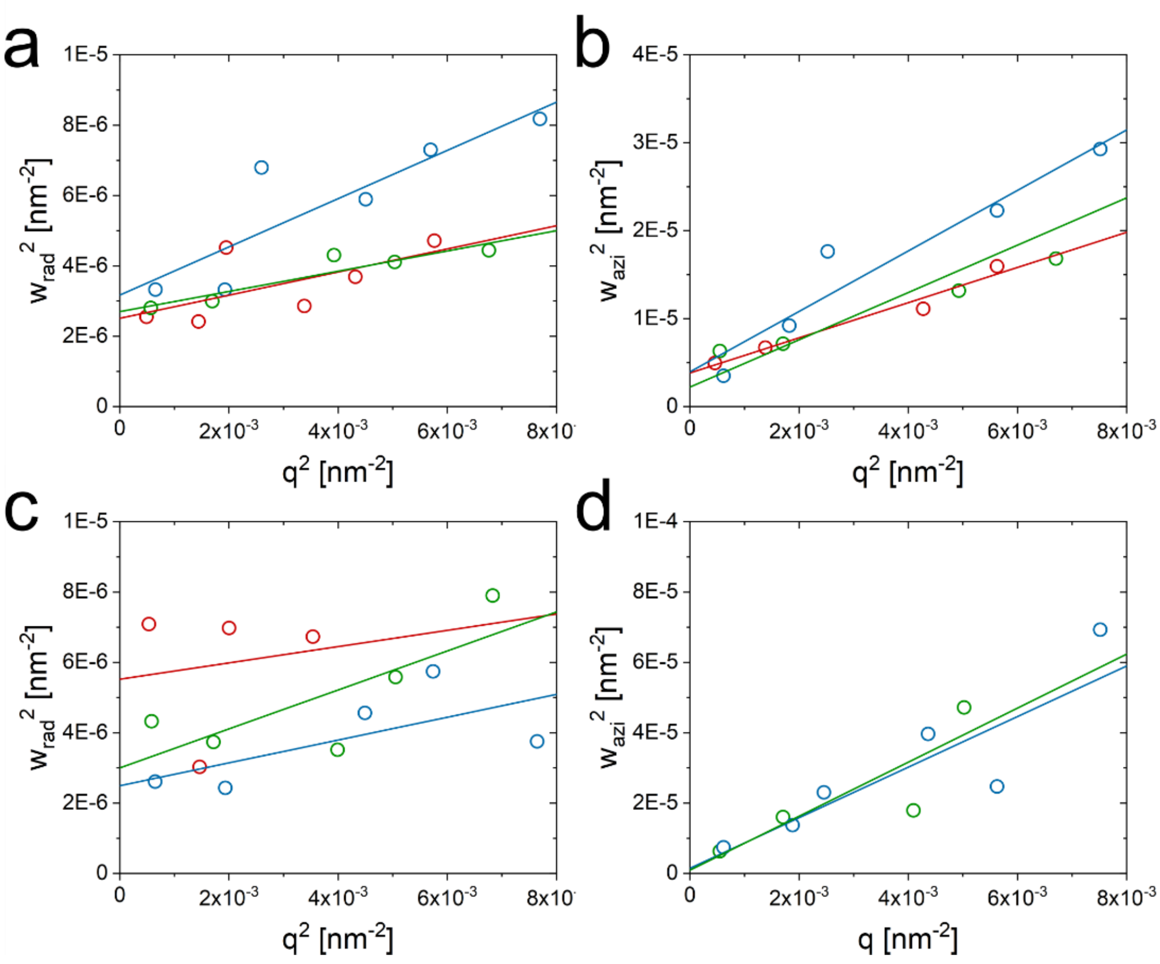

Figure S7. Williamson-Hall analysis. The square of the FWHM of the Bragg peaks in radial and azimuthal orientation as function of q^2. Data obtained from ζ = 0.56 CS microgel dispersions is shown in red, green corresponds to 0.70 and blue to 0.84 respectively unscreened (**a**, **b**) and charge-screened state (**c**, **d**). The straight lines represent the linear fits applied to the data. ζ is calculated based on number concentration *N* and the hydrodynamic radius at 20 °C in the salt-free state. Data from samples in the salt-free state is adapted from our previous work.[1]

The small slopes extracted from the Williamson-Hall analysis indicate only weak strains in our colloidal crystals and the intercepts used to calculate the size of the coherently scattering domains are listed in **Table S10** and **Table S11**.

Table S10. Parameters from linear fits in Williamson-Hall analysis for CS microgels in absence of salt. Adapted from our previous work.[1]

ζ (20 °C)	**Intercept (rad.) [nm^{-2}]**	**Slope (rad.)**	**Intercept (azi.) [nm^{-2}]**	**slope (azi.)**
0.56	2.5E-6	3.3E-4	3.8E-6	2.0E-3
0.70	2.7E-6	2.9E-4	2.2E-6	2.7E-3
0.84	3.2E-6	6.9E-4	3.9E-6	3.4E-3

Table S11. Parameters from linear fits in Williamson-Hall analysis for CS microgels in the charge-screened state. ζ is calculated based on number concentration N and the hydrodynamic radius at 20 °C in the salt-free state.

ζ (20 °C)	**Intercept (rad.) [nm^{-2}]**	**Slope (rad.)**	**Intercept (azi.) [nm^{-2}]**	**slope (azi.)**
0.56	5.5E-6	2.3E-4	-	-
0.70	3.0E-6	5.5E-4	1.5E-6	7.2E-3
0.84	2.5E-6	3.2E-4	9.2E-7	3.2E-4

Figure S8 shows the radial and azimuthal coherently scattering domain sizes in dependence of ζ and charge screening extracted from the Williamson-Hall analysis. We found domain sizes between 2 and 4 µm. Azimuthal domain sizes in presence of salt possess large error bares in combination with exceptional large domain sizes, which indicates that the Williamson-Hall analysis might be not applicable on the respective scattering patterns.

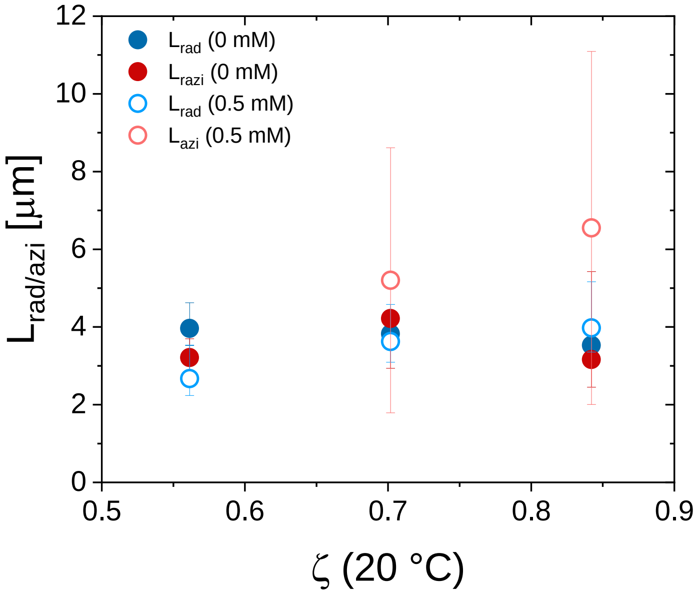

Figure S8. Radial and azimuthal coherently scattering domain sizes. Data from samples in the salt-free state is adapted from our previous work.[1]

Absorbance Spectroscopy of CS microgels in Dense Packings

In **Figure S9** we want to compare the Vis-NIR absorbance spectra recorded from CS microgels in dense packing used for the SAXS experiments and for temperature dependent absorbance spectroscopy. Nearly all spectra show narrow Bragg peaks indicating the presence of crystalline structures. The samples at ζ (20 °C) = 0.42 (orange) in **Figure S9a** and ζ = 0.49 in the charge-screened state (grey) in **Figure S9b** show no Bragg peaks. In general, for higher volume fractions the Bragg peaks shift towards lower wavelength. This reflects the decrease in the lattice constant *a* of the colloidal crystals presented in **Table S12** and **S13**.

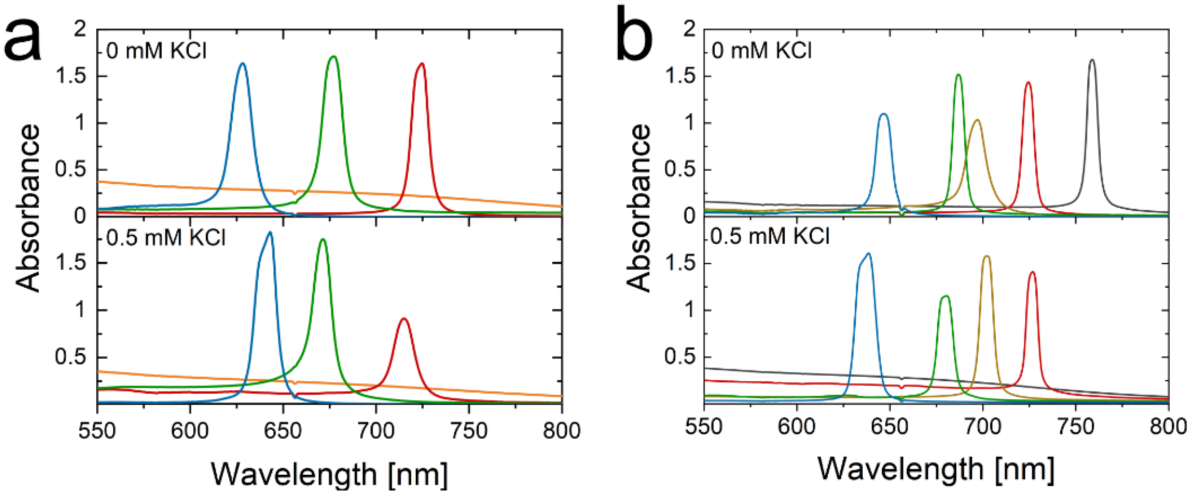

Figure S9. Vis-NIR absorbance spectra of CS microgels in dense packing in absence and presence of salt after thermal treatment. The dispersions exhibit generalized volume fractions ζ (20 °C) of 0.42 (orange), 0.49 (grey), 0.56 (red), 0.63 (dark orange), 0.70 (green) and 0.84 (blue). Spectra were recorded at a temperature of 20 °C. (**a**) CS microgel dispersions used for SAXS experiments and (**b**) for temperature dependent absorbance spectroscopy. ζ (20 °C) is calculated based on number concentration N and the hydrodynamic radius at 20 °C in the salt-free state. Data from samples prepared without the addition of salt presented in (**a**) is adapted from our previous work.[1]

For all CS microgel dispersions possessing the same ζ, we find similar Bragg peak positions. Only for the ζ being 0.84 (**Figure S9a**) we find a larger deviation of 20 nm between Peak positions. In terms of the lattice constant this translates to a deviation of 3% and we ascribe this to an imperfect formation of the crystalline structures in the respective probed volume. Bragg peak positions and the respective lattice constants *a* are given in **Table S12** (**Figure S9a**) and **Table S13** (**Figure S9b**).

Table S12. Bragg peak position and respective lattice constants for the hcp crystal structure obtained from the absorbance spectra of the CS microgel samples used for SAXS experiments. *ζ* (20 °C) is calculated based on number concentration *N* and the hydrodynamic radius at 20 °C in the salt-free state. Data recorded in absence of salt is adapted from our previous work.[1]

***ζ* (20 °C)**	**c_{KCl} [mM]**	**Bragg peak [nm]**	**Lattice constant *a* [nm]**
0.42	0	-	-
0.42	0.5	-	-
0.56	0	724	329
0.56	0.5	715	325
0.70	0	676	308
0.70	0.5	671	305
0.84	0	628	286
0.84	0.5	641	292

Table S13. Bragg peak position and respective lattice constants for the hcp crystal structure of obtained from the absorbance spectra of the CS microgel samples used for temperature dependent absorbance spectroscopy. *ζ* (20 °C) is calculated based on number concentration *N* and the hydrodynamic radius at 20 °C in the salt-free state.

***ζ* (20 °C)**	**c_{KCl} [mM]**	**Bragg peak [nm]**	**Lattice constant *a* [nm]**
0.49	0	759	346
0.49	0.5	-	-
0.56	0	724	330
0.56	0.5	726	331
0.63	0	696	317
0.63	0.5	702	320
0.70	0	687	313
0.70	0.5	680	310
0.84	0	647	295
0.84	0.5	637	290

Phase Transitions Followed by Temperature-Dependent Spectroscopy

Phase transitions between crystalline and fluid states in dispersions of CS microgels at dense packings are followed by the temperature-dependent absorbance of the Bragg peaks. Here, we recoded Vis-NIR absorbance spectra between 20 °C and 50 °C in 0.3 °C steps with equilibration times of 720 s. The samples were prepared in absence and presence of KCl. For an increase in temperature, a decrease in the Bragg peak intensity followed by a complete disappearance can be monitored for all samples. The same trend in reverse can be found for the cooling process where the Bragg peak reappears and increases in intensity. Here we want to note that the presence of a Bragg peak is a clear indicator for the presence of crystalline structures in the probed volume but does not generally exclude the co-existence with a fluid subphase. Nevertheless, fluid subphases can be neglected for higher volume fractions as their presence is not indicated by SAXS for $\zeta > 0.56$. **Figure S10** and **Figure S11** show the temperature-dependent absorbance spectra as well as the background corrected absorbance of the Bragg peaks as function of temperature. The green areas indicate the respective temperature ranges, where the CS microgels undergo the transition between the crystalline and fluid state. In general, we can detect some minor changes of the Bragg peak position and intensity before and after the temperature-dependent measurements. We associate this to small changes in the unit cell dimensions and long-range order of the colloidal crystals in the probed sample volume.

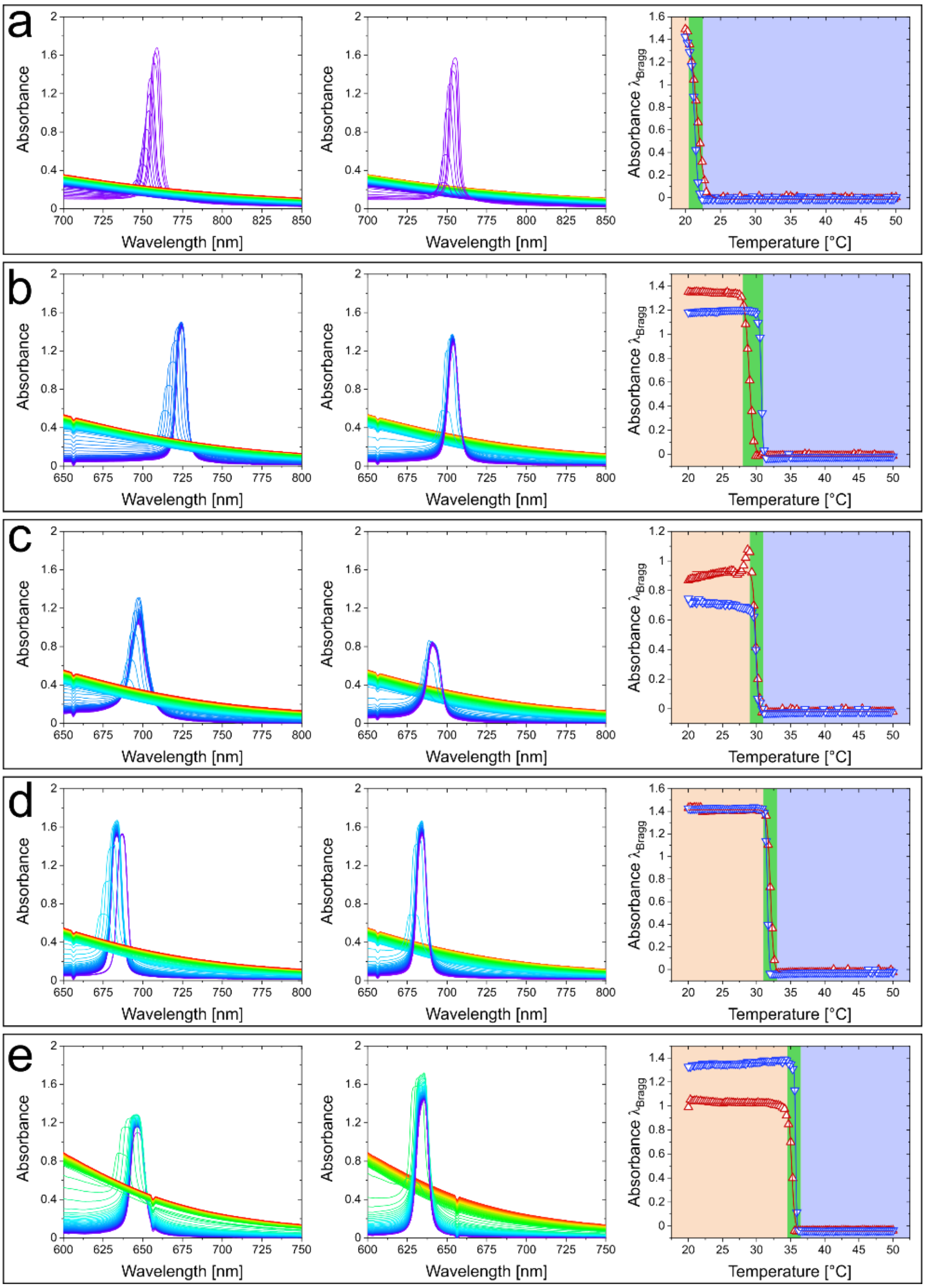

Figure S10. Temperature-dependent Vis-NIR absorbance spectra of the CS microgel dispersions for the heating and cooling process as well as the background corrected absorbance of the Bragg peak as function of temperature. The color transition from blue to red indicates the change in temperature and the red and blue triangles correspond to the heating and cooling process. Here, the solid red and blue lines are sigmoidal fits indicating the course of the transition of the Bragg peak absorbance. Spectra were recorded of CS microgel dispersions with ζ (20 °C) of (**a**) 0.49, (**b**) 0.56, (**c**) 0.63, (**d**) 0.70 and (**e**) 0.84 in the absence of salt.

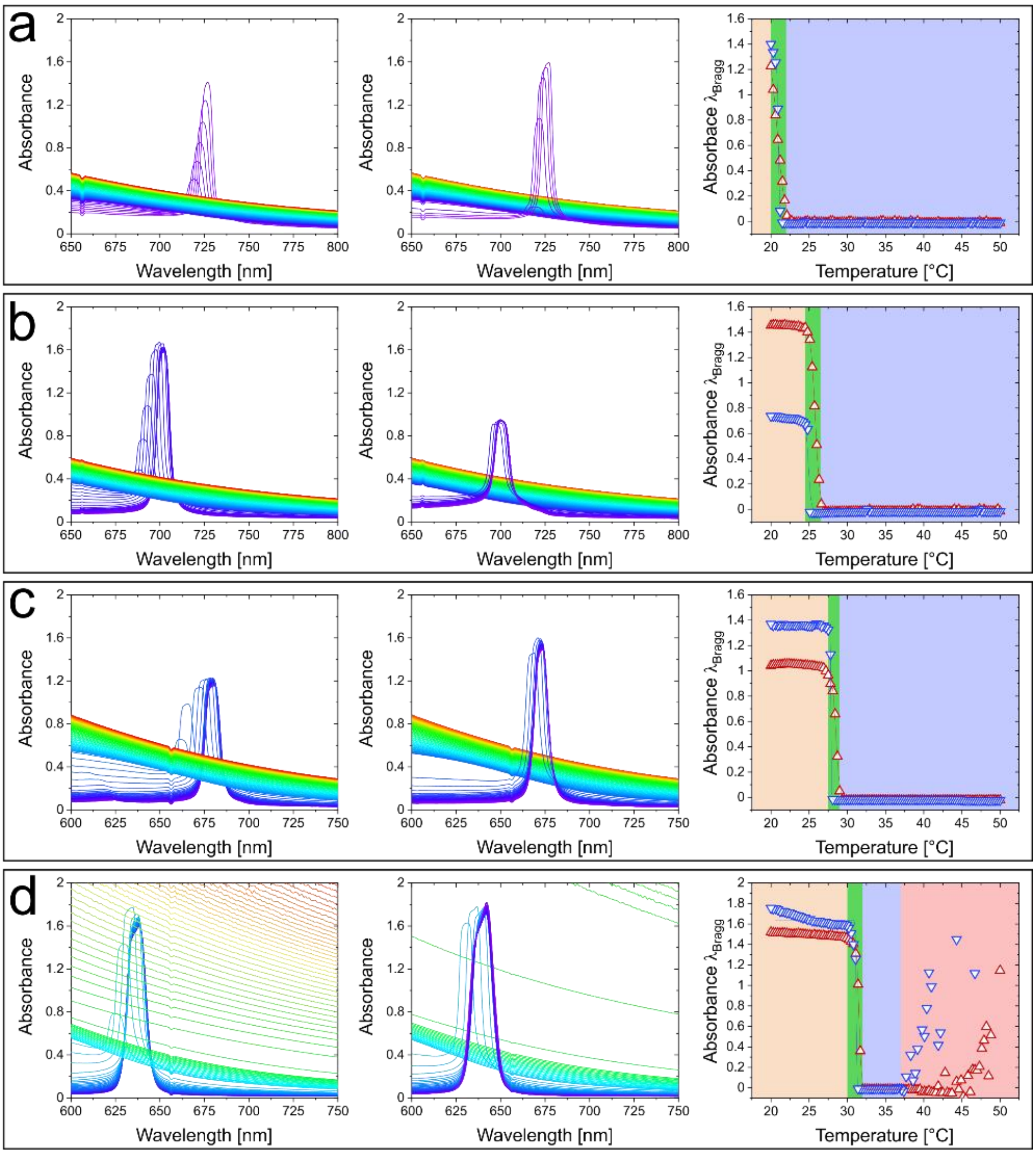

Figure S11. Temperature-dependent Vis-NIR absorbance spectra of the CS microgel dispersions for the heating and cooling process as well as the background corrected absorbance of the Bragg peak as function of temperature. The color transition from blue to red indicates the change in temperature and the red and blue triangles correspond to the heating and cooling process. Here, the solid red and blue lines are sigmoidal fits indicating the course of the transition of the Bragg peak absorbance. Spectra were recorded of CS microgel dispersions with ζ (20 °C) of (**a**) 0.56, (**b**) 0.63 (**c**) 0.70 and (**d**) 0.84 in the charge-screened state. ζ (20 °C) is calculated based on number concentration N and the hydrodynamic radius at 20°C for the salt-free state.

The general temperature-dependent behavior of the CS microgel dispersions prepared in absence and presence of salt is very similar. When reaching a specific temperature, the Bragg peak intensity decreases until the Bragg peak disappeared. The process is reversible when the temperature is decreased again. In comparison to the salt-free state, dispersions in the charge-screened state exhibit a shift of the transition temperature towards lower temperatures. The Vis-NIR absorbance spectra in **Figure S11d**, correspond to ζ (20 °C) = 0.84 in the charge-screened state exhibit a strong increase in absorbance after the phase transition, indicated in red. This behavior was not observed for any other sample, and we conclude that the presence of KCl in combination with the volume fraction enabled aggregation of the CS microgels above a certain temperature. The aggregation of the microgels would lead to larger scattering objects followed by an increase in light scattering of the sample. In absorbance spectroscopy an increase in the scattering contribution of the sample would lead to an increase in absorbance as less light being able to pass through the sample. This can be seen in **Figure S12** where the absorbance at the wavelength of 700 nm is presented as function of temperature. The absorbance increases above a temperature of 36 °C for the heating and cooling procedure until it reaches the instrumental limitations around a value of 3.5.

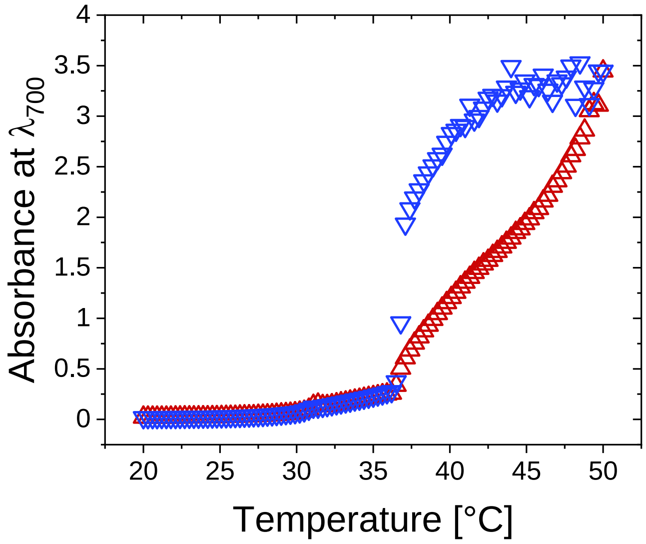

Figure S12. Temperature-dependent absorbance at the wavelength of 700 nm for ζ (20 °C) = 0.84 CS microgel dispersion in the charge-screened state. Red corresponds to the heating and blue to the cooling process.

Temperature-dependent Vis-NIR spectroscopy enables the determination of the phase transition temperature between the crystalline- and fluid state of the CS microgel dispersions, in dependence of ζ (20 °C). From temperature dependent DLS we know R_h at these transition temperatures and are able to calculate the respective volume of the CS microgels. In combination with particle number concentration N, extracted from the scattering intensity of the SiO_2 cores, we can calculate the generalized volume fraction ($\zeta_{\text{transition}}$) for the transition process. $\zeta_{\text{transition}}$ in absence (full circles) and presence (open circles) of salt as function of ζ (20 °C) is shown in **Figure S13a.** The heating and cooling processes are indicated by red and blue symbols. It is clearly shown that the screening of charges increases $\zeta_{\text{transition}}$ from a value of 0.43 ± 0.03 (c_{KCl} = 0 mM) to 0.54 ± 0.02 (c_{KCl} = 0.5 mM). The shift of $\zeta_{\text{transition}}$ is attributed to a reduction of the effective electrostatic interaction radius between the CS microgels, due to screened charges in the presence of additional ions. This is in good agreement with the results from the structure factor analysis (SAXS) of the CS microgels in the fluid state at 40 °C. Based on the following equation, under the assumption that the CS microgels crystallize similar to hard spheres, at a volume fraction of 0.494[11], we were able to calculate an effective hard sphere radius of the microgels:

$$R_{\text{hard sphere}} = \frac{\left(\frac{\zeta_{\text{transition}} R_{\text{h,transition}}{}^{-3}}{0.494}\right)^{-\frac{1}{3}}}{R_{\text{h,transition}}} R_{\text{h,20 °C}} \qquad \text{(S10)}$$

The effective hard sphere radius is $R_{\text{hard sphere}}$ and $R_{\text{h, transition}}$ corresponds to the hydrodynamic radius at the transition temperature. The calculated effective hard sphere radii are shown in **Figure S13b**. Similar to $\zeta_{\text{transition}}$ we detect a distinct influence of the charge screening, as the effective hard sphere radius deceases from 154 for the salt-free state to 143 nm in the screened state. An influence of ζ (20 °C) on $\zeta_{\text{transition}}$ and the effective hard sphere radius was not found. This might be attributed to the fact, that the here performed calculations are based on $R_h(T)$ and potential osmotic deswelling or changes of the ionic strength of the dispersion due to an increase in microgel concentration could not be addressed.

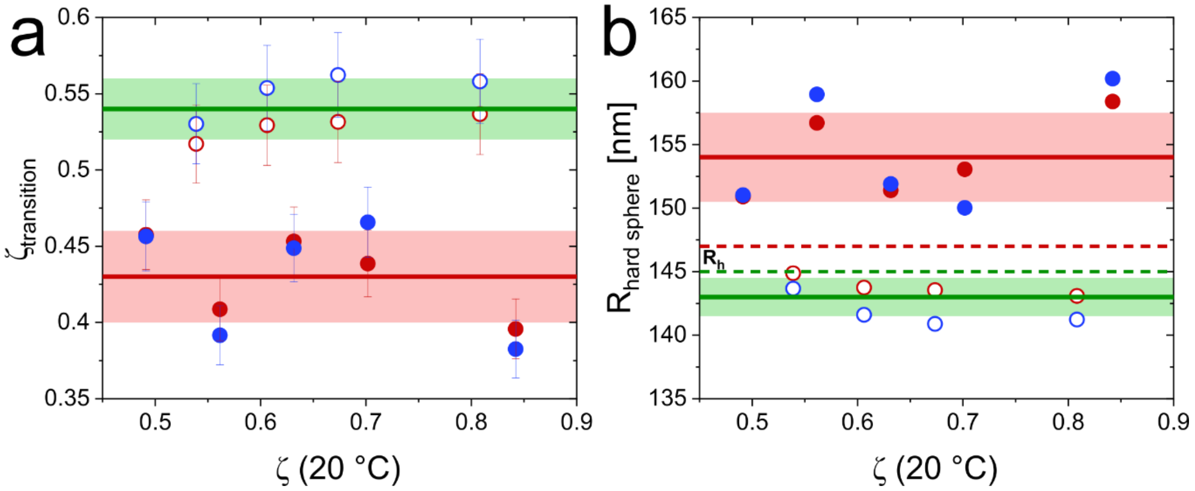

Figure S13. Transition volume fraction and corresponding hard sphere mapping. Full circles correspond to dispersions in absence of salt and empty circle correspond to samples in the charge-screened state. The melting and recrystallization process are indicated by the red and blue color of the symbols. (**a**) Generalized volume fraction $\zeta_{\text{transition}}$ of the CS microgel dispersions regarding the transition between fluid and crystalline regime in dependence of ζ (20 °C). The straight lines indicate the average $\zeta_{\text{transition}}$, red for the absence of salt and green for the charge-screened state. The colored area displays the respective standard deviation. (**b**) Hard sphere radius of the CS microgels as function of ζ (20 °C). Assuming that the CS microgels would actually crystallize similar to hard spheres at a volume fraction of 0.494. The straight lines indicate the average hard sphere radius, red for the absence of salt and green for the charge-screened state. The colored area displays the standard deviation and the dashed lines correspond to the respective R_{h}'s at 20 °C.

Characterization of Core-Shell Microgel 2 (CS2)

In terms of recording a temperature-dependent phase diagram of the CS microgels in dense packing a second batch of CS microgels (CS2) was synthesized. The synthesis was performed similar to the one of the CS microgels used in this and our previous work[1], but upscaled to yield a higher mass of particles. 7500 mg *N*-isopropylacrylamide (NIPAM, TCI, >98%) and 1535 mg *N*,*N'*-methylenebis(acrylamide) (BIS, Sigma-Aldrich, 99%) were dissolved in 1500 mL of ultra pure water (18.2 MΩcm). 300 mg of 3-(trimethoxysilyl)propyl methacrylate (MPS, Sigma Aldrich, 98%) functionalized SiO_2 particles[4] were added to the solution, which was flushed with argon for 2 h at a temperature of 70 °C. The reaction was initiated with 75 mg potassium persulfate (PPS, Sigma-Aldrich, 99,0%) dissolved in 2 ml water and stopped after 4 h. All chemicals were used as received without further purification.

The core-shell nature of the microgels is shown in the TEM images of CS2 in **Figure S14a** and **b**. Only a minor fraction of particles below 1% does not possess a SiO_2 core. One example is indicated by a red circle in **Figure S14b**. The size distribution of the cores, based on TEM image analysis, is shown in **Figure S14c** resulting in an average R_{TEM} = 20 ± 1 nm. **Figure S14d** shows the R_h of CS2 as function of temperature in absence (red) and presence of salt (orange). Hydrodynamic radii of CS1 and CS2 at 20 °C and 40 °C are given in **Tables S6** and **S18**. Compared to CS1 in terms of R_h (147 nm and 149 nm at 20 °C), core size (18 nm and 20 nm) and the nominal crosslinker ratio (15% for both), the CS2 microgels are an ideal system to perform additional experiments with, while maintaining a direct comparability between the two microgel systems. Even in terms of their electrophoretic mobility, the CS2 microgels show nearly the same mobilities in dependence of temperature and charge screening as shown in **Figure S14e**.

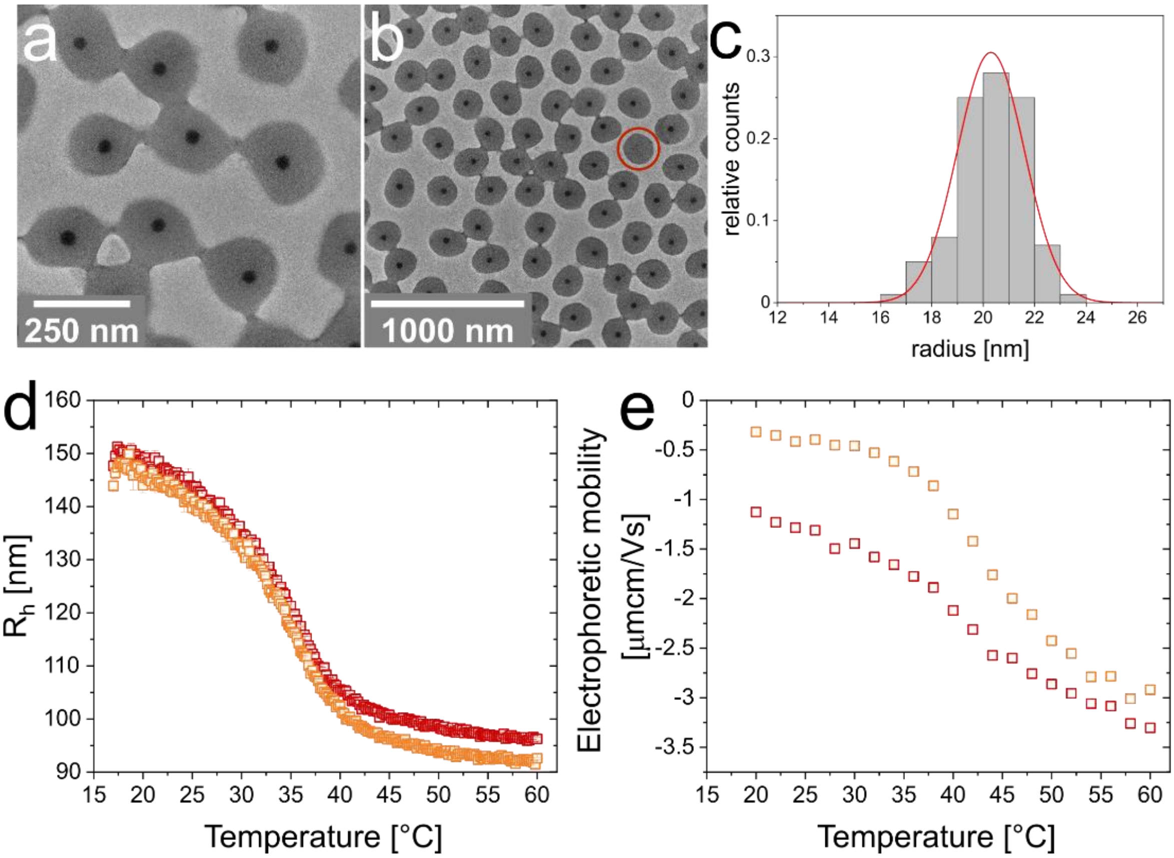

Figure S14. Characterization of CS2. (**a**, **b**) TEM images at different magnifications. The red circle indicates a single microgel without a core. (**c**) Size distribution of the SiO_2 cores from TEM image analysis. (**d**) R_h of CS2 as function of temperature in absence of salt (red squares) and in the charge-screened state (orange squares). (**e**) Electrophoretic mobility as function of temperature. Same color coding as in (**d**).

Extraction of Number Concentration for CS2

We determined the relation between particle number concentration *N* and the mass content of the CS microgel dispersion, based on the scattering intensity of the SiO_2 cores in SAXS at infinitely small *q* (I_0), following our previous works.[1, 5] We recorded the scattering profiles of three dispersions of CS2 microgels with mass contents of 10 wt% and performed form factor analysis on the scattering data. Here, we focused on the *q*-regime where the scattering of the core dominates the SAXS profile and applied a simple hard sphere model fit, resulting in R_{SAXS} of 20 ± 2 nm. The scattering profiles and respective form factor fits are shown in **Figure S15a**. Parameters applied to fit the scattering profiles are listed in **Table S14**. For the extraction of I_0 we performed a Guinier analysis on the plateau-like regime of the scattering profile in the low *q* regime (**Figure S15b**).

The scattering in the respective *q*-range already exhibits contributions of the shell and is not solely obtained from the SiO_2 core. Therefore, we also performed the Guinier-analysis on the form factor fits (**Figure S15c**). With this approach, we verify that the scattering of the shell does not influence our final results. Nevertheless, the data obtained from both approaches is listed in **Table S15** and **S16**.

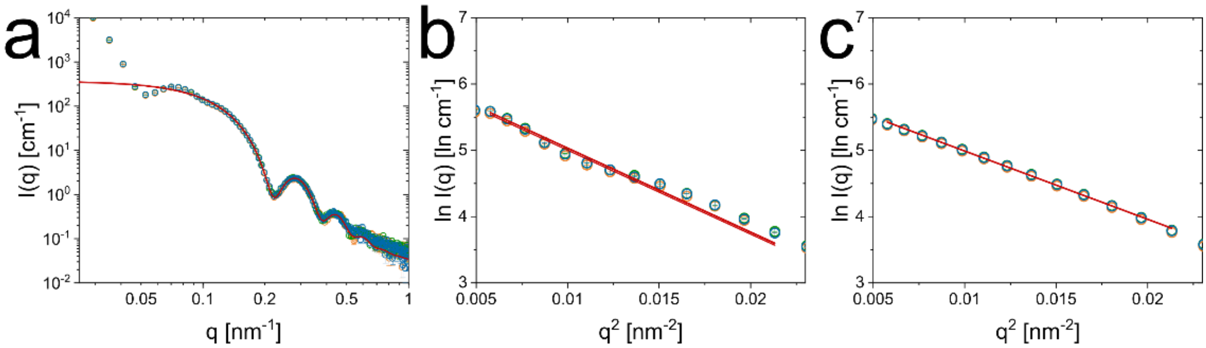

Figure S15. Extraction of the particle number concentration *N*. (**a**) Scattering profiles of three 10 wt% CS microgel dispersions. The solid red lines correspond to form factor fits describing the scattering of the SiO_2 core (**Equation S5**). Guinier plots of the scattering data (**b**) and the respective form factor fits (**c**). The solid red lines indicate the linear fits applied to the data.

Table S14. Fit parameters obtained from the form factor fits (polydisperse sphere model). The Errors of the parameters are smaller by two orders of magnitudes compared to the obtained valuers and therefore not listed.

	I	II	III
scale	0.00145	0.00150	0.00149
I_B [cm^{-1}]	0.03	0.03	0.03
SLD (SiO_2) [10^{-6} Å^{-2}]	17.8	17.8	17.8
SLD (H_2O) [10^{-6} Å^{-2}]	9.5	9.5	9.5
R [nm]	20	20	20
σ_{poly}	0.08	0.08	0.08

Table S15. Results from Guinier analysis of the SAXS data.

	I	II	III
I_0 [cm^{-1}]	528 ± 24	546 ± 26	543 ± 26
R_g [nm]	19.5 ± 0.4	19.5 ± 0.4	19.5 ± 0.4

Table S16. Results from the linear fits applied on the Guinier plots of the form factor fits.

	I	II	III
I_0 [cm^{-1}]	404 ± 6	413 ± 6	410 ± 6
R_g [nm]	17.6 ± 0.1	17.6 ± 0.1	17.6 ± 0.1

Similar to our previous work, we yield a lower I_0 from the Guinier analysis of the form factor fits compared to the analysis performed on the scattering data. In addition, the R_g extracted from the form factor fits is closer to the expected value for R_g according to $R_g = \sqrt{\frac{3}{5}}\, R_{P(q)} = 15.5$ nm. In order to avoid the scattering of the shell, influencing the determination of the particle number concentration N, we used the results from the Guinier analysis of the form factor fits for further calculations.

The particle number concentration N can be calculated by the following equation:

$$N = \frac{I_0\, N_A\, \rho^2}{m\, M_w\, \Delta SLD^2} \qquad \text{(S11)}$$

Here, N_A is Avogadro's number, ρ is the density of the silica cores, the mass of a single scattering object, m, M_w being the molecular weight, of the scattering object, and ΔSLD

related to the difference in scattering length density between the solvent and the scattering object. We find an average particle number concentration N of $5.21 \cdot 10^{12}$ $wt\%^{-1}mL^{-1}$ for the CS2 microgels (**Table S17**), this is nearly the same relation as for CS1 ($N = 5.27 \cdot 10^{12}$ $wt\%^{-1}mL^{-1}$).[1]

Table S17. Number concentrations extracted from the scattering intensity of CS2 microgel dispersions (10wt%).

	I	II	III	$\bar{N}$	*SD*
N ($I(q)$) [10^{13} 1/mL]	6.73	6.96	6.92	6.87	0.10
N ($P(q)$) [10^{13} 1/mL]	5.15	5.26	5.22	5.21	0.05

Generalized volume fractions (ζ) in presence and absence of salt at temperatures of 20 °C and 40 °C for the CS2 microgels are given in **Tables S18**. Here, ζ is calculated based on particle number concentrations N and the respective R_h.

Table S18. R_h and the respective selected ζ for CS2 microgels at 20 °C and 40 °C in absence of salt and in the charge-screened state.

T = 20 °C **c_{KCl} = 0 mM**	**T = 20 °C** **c_{KCl} = 0.5 mM**	**T = 40 °C** **c_{KCl} = 0 mM**	**T = 40 °C** **c_{KCl} = 0.5 mM**
149 nm	144 nm	106 nm	102 nm
0.43	0.39	0.16	0.14
0.58	0.52	0.21	0.19
0.72	0.65	0.26	0.23
0.87	0.78	0.31	0.28

Vis-NIR Absorbance Spectroscopy for the Preparation of the Phase Diagrams

Absorbance spectra of the CS2 microgel dispersions before (a) and after annealing (b) are shown in **Figure S16.** In accordance to our previous work,[1] the annealing procedure increased the intensity and decreased the width of the Bragg peaks. For more details we refer to the respective Supporting Information. After the annealing procedure, the spectra express similar trends compared to the spectra recorded from the CS1 system. Here, Bragg peaks were detected from samples with ζ(20 °C) of 0.32

in the salt-free state. This is a much lower volume fraction than expected, based on the results from the CS1 microgel system. When charges are screened, a ζ(20 °C) of 0.51 is needed for the CS2 microgel dispersions to exhibit Bragg peaks, which is in good agreement with the previous results for the CS1 microgels. We performed temperature dependent Vis-NIR spectroscopy on samples in a range of ζ from 0.32 to 1.20 for CS microgels in the absence of salt and from 0.55 to 1.06 under charge-screened conditions. Here, the 1.20 and 1.06 CS2 microgel dispersions in the unscreened and screened state, respectively, possess the same particle number concentration N. The reason for the difference in ζ(20 °C) is the slightly smaller R_h recorded under charge-screened conditions, which was used to calculate ζ. A comparison of selected values of ζ and the respective R_h's at 20 and 40 °C in absence and presence of KCl is given in **Table S11**.

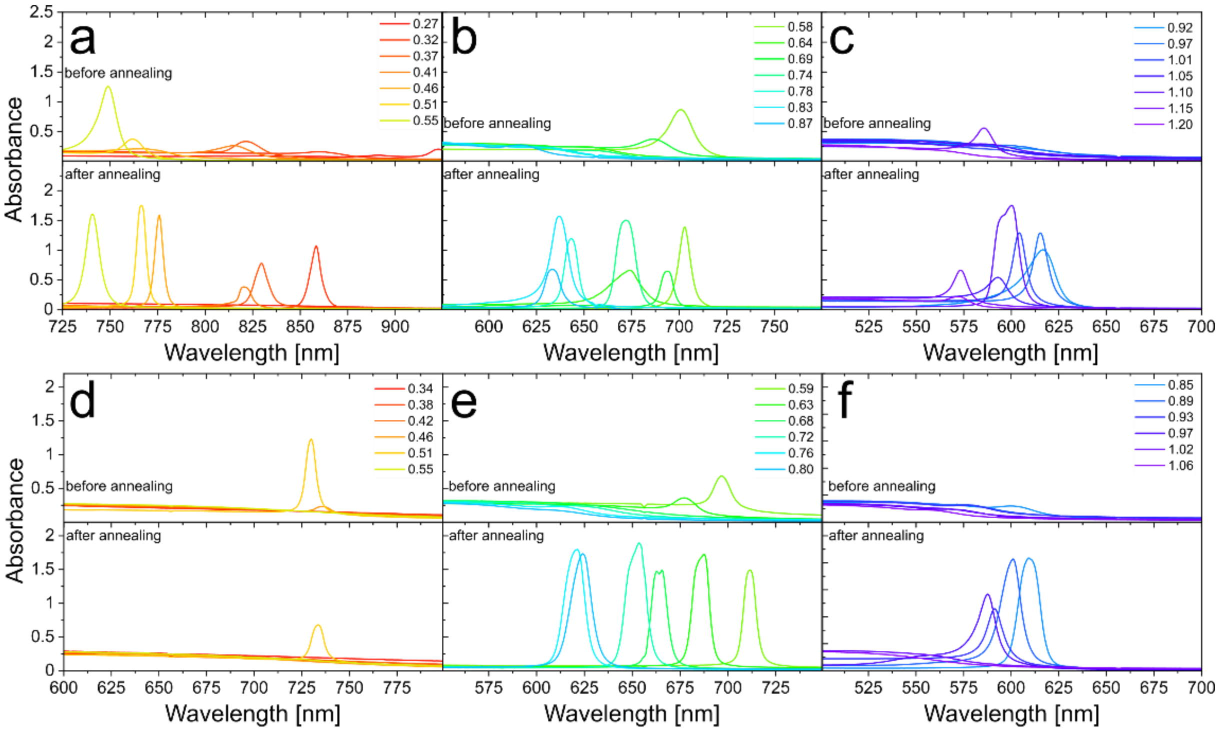

Figure S16. Vis-NIR absorbance spectra of CS2 microgels before and after the annealing process over a broad range of generalized volume fractions ζ, for c_{KCl} = 0 mM (top, **a**, **b**, **c**) and c_{KCl} = 0.5 mM (bottom, **d**, **e**, **f**) recorded at a temperature of 20 °C.

Temperature-dependent Vis-NIR spectroscopy was performed on samples shown in **Figure S16**. The transition temperatures between the fluid and crystalline state were extracted similar to the CS1 microgels and are shown in **Figure S17a** and **S17b**. As expected, the transition temperature increases for higher ζ and the addition of KCl to the microgel dispersion lowers the transition temperature for the respective ζ compared to the CS microgels in the salt-free state.

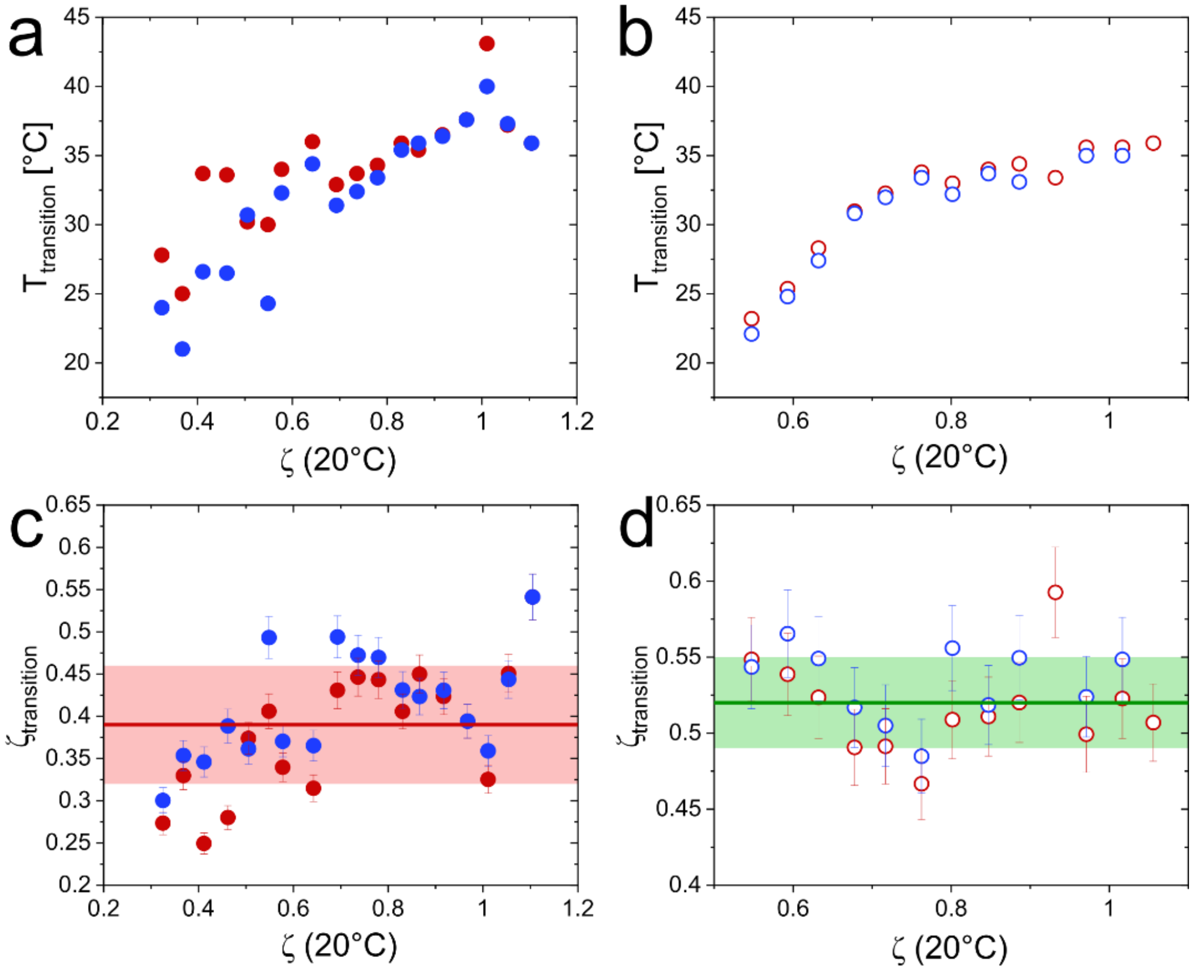

Figure S17. Transition temperature between the fluid and crystalline state for CS2 microgel dispersions in absence of salt (**a**) and in the charged-screened state (**b**). The temperature is given in dependence of the generalized volume fraction ζ, extracted from temperature dependent Vis-NIR absorbance spectra. $\zeta_{transition}$ as function of ζ(20 °C) in absence of salt (**c**) and in the charged-screened state (**d**). The sloid lines indicate the average $\zeta_{transition}$ and the colored area corresponds to the respective standard deviation. Red symbols refer to the heating and blue symbols to the cooling process.

Based on the transition temperature, the respective R_h and particle number concentration N, we can calculate $\zeta_{transition}$ for the CS2 system at in absence of salt and in the charge-screened state shown in **Figure S17c** and **S17d**. The average $\zeta_{transition}$, indicated by the solid line, is 0.39 ± 0.07 for the salt-free state and 0.52 ± 0.03 in presence of salt. The transition volume fractions extracted from temperature dependent Vis-NIR absorbance spectroscopy on CS2 microgel dispersions yield nearly the same results compared to the CS1 microgel system (c_{KCl} = 0 mM: 0.43 ± 0.03; c_{KCl} = 0.5 mM: 0.54 ± 0.02). Comparing two very similar but different batches of

CS microgels and yielding nearly the same average $\zeta_{\mathrm{transition}}$ underlines the reliability of the applied method.

References

1 M. Hildebrandt, D. Pham Thuy, J. Kippenberger, T. L. Wigger, J. E. Houston, A. Scotti and M. Karg, *Soft Matter*, 2023, **19**, 7122-7135.

2 L. A. Feigin and D. I. Svergun, *Structure Analysis by Small-Angle X-ray and Neutron Scattering*, Springer New York, NY, 1987.

3 SasView, http://www.sasview.org/.

4 K. D. Hartlen, A. P. T. Athanasopoulos and V. Kitaev, *Langmuir*, 2008, **24**, 1714-1720.

5 M. Hildebrandt, S. Lazarev, J. Pérez, I. A. Vartanyants, J. M. Meijer and M. Karg, *Macromolecules*, 2022, **55**, 2959-2969.

6 J. K. Percus and G. J. Yevick, *Phys Rev*, 1958, **110**, 1-13.

7 J. B. Hayter and J. Penfold, *Mol Phys*, 1981, **42**, 109-118.

8 Y. Liu, W. R. Chen and S. H. Chen, *J Chem Phys*, 2005, **122**.

9 M. Heinen, P. Holmqvist, A. J. Banchio and G. Nägele, *J Chem Phys*, 2011, **134**, 044532.

10 J. Kohlbrecher and I. Bressler, *J Appl Crystallogr*, 2022, **55**, 1677-1688.

11 P. N. Pusey and W. Van Megen, *Nature*, 1986, **320**, 340-342.